Mode-I crack in a two-dimensional fibre-reinforced generalized thermoelastic problem

Kh. Lotfy

Department of Mathematics, Faculty of Science, Zagazig University, Zagazig P.O. Box 44519, *Egypt*
Department of Mathematics, Faculty of Science and Arts, Al-mithnab, Qassim University, P.O. Box 931, *Buridah* 51931, *Al-mithnab, Kingdom of Saudi Arabia*

(Received 3 April 2011; revised manuscript received 30 June 2011)

A general model of the equations of the Lord–Şulman theory including one relaxation time and the Green–Lindsay theory with two relaxation times, as well as the classical dynamical coupled theory, are applied to the study of the influence of reinforcement on the total deformation for an infinite space weakened by a finite linear opening mode-I crack. We study the influence of reinforcement on the total deformation of rotating thermoelastic half-space and their interaction with each other. The material is homogeneous isotropic elastic half space. The crack is subjected to prescribed temperature and stress distributions. The normal mode analysis is used to obtain the exact expressions for displacement components, force stresses, and temperature. The variations of the considered variables with the horizontal distance are illustrated graphically. Comparisons are made with the results obtained in the three theories with and without rotation. A comparison is also made between the two theories for different depths.

Keywords: mode-I crack, Lord–Şulman theory, thermoelasticity, normal mode analysis.

PACS: 42.65.Hf **DOI:** 10.1088/1674-1056/21/1/014209

1. Introduction

The linear theory of elasticity is of paramount importance in the stress analysis of steel, which is the most common engineering structural material. To a lesser extent, linear elasticity describes the mechanical behaviour of other common solid materials, e.g., concrete, wood, and coal. However, the theory does not apply to the behaviour of many new synthetic materials of the clastomer and polymer type, e.g., polymethyl-methacrylate (Perspex), polyethylene, and polyvinyl chloride.

For ultrasonic waves, i.e., for the case of elastic vibrations characterized by high frequencies and small wavelengths, the influence of the body microstructure becomes significant. Metals, polymers, composites, solids, rocks, and concrete are typical media with microstructures. More generally, most natural and manmade materials including engineering, geological, and biological media possess microstructures. The influence of the microstructure results in the development of new types of waves, which are not described in the classical theory of elasticity. A reinforced concrete member shall be designed for all conditions of stresses that may occur, and should be in accord with the principle of mechanics.

Fibre-reinforced composites are used in a variety of structures due to their low weight and high strength. The characteristic property of a reinforced composite is that its components act together as a single anisotropic unit as long as they remain in the elastic condition. The wave propagation in reinforced media plays a very interesting role in civil engineering and geophysics. The study of the propagation, reflection, and transmission of waves is of great interest to seismologists. Such studies help them to obtain a rock's structure as well as its elastic properties, and the information regarding minerals and fluids present inside the earth. The idea of introducing a continuous self reinforcement at every point of an elastic solid was given by Belfied *et al.*[1] The model was later applied to the rotation of a tube by Verma and Rana.[2] Verma[3] has also discussed magneto elastic shear waves in self-reinforced bodies. Singh[4] showed that for wave propagation in fibre-reinforced anisotropic media, the decoupling can not be achieved by the introduction of the displacement potential. Sengupta and Nath[5] discussed the problem of surface waves in fibre-reinforced anisotropic elastic media. Hashin and Rosen[6] gave the elastic moduli for fibre-reinforced materials. The problem of the re-

†Corresponding author. E-mail: khlotfy_1@yahoo.com
© 2012 Chinese Physical Society and IOP Publishing Ltd

flection of plane waves at the free surface of a fibre-reinforced elastic half-space was discussed by Singh *et al.*[7] Chattopadhyay and Choudhury[8] have discussed the problem of propagation, reflection, and transmission of magneto elastic shear waves in a self–reinforced medium. The reflection and the transmission of a plane SH wave through a self-reinforced elastic layer sandwiched between two homogeneous visco-elastic solid half-spaces have been studied by Chaudhary *et al.*[9] Chattopadhyay and Chaudhury[10] studied the propagation of magneto-elastic shear waves in an infinite self-reinforced plate. Pradhan *et al.*[11] studied the dispersion of Loves waves in a self-reinforced layer over an elastic non-homogenous half space. The propagation of plane waves in fibre-reinforced media was discussed by Chattopadhyay *et al.*[12]

The theory of coupled thermo-elasticity was extended by Lord and Şhulman[13] and Green and Lindsay[14] by including the thermal relaxation time in the constitutive relations. Those two theories eliminate the paradox of the infinite velocity of heat propagation and are termed generalized theories of thermoelasticity. There exist the following differences between the two theories: i) the Lord–Şulman (L–S) theory involves one relaxation time of thermoelastic process (τ_0). The Green and Lindsay (G–L) theory involves two relaxation times (τ_0, ν_0). ii) The L–S energy equation involves first and second time derivatives of the strain, whereas the corresponding equation in the G–L theory needs only the first time derivative of the strain. iii) In the linearized case, according to the approach of the G–L theory, heat cannot propagate with a finite speed unless the stresses depend on the temperature velocity, whereas according to the L–S theory, heat can propagate with a finite speed even though the stresses there are independent of the temperature velocity. iv) The L–S theory can not be obtained from the G–L theory.

Choudhuri and Debnath[15,16] and Othman[17−20] studied the effect of rotation in a micropolar generalized thermoelastic and thermo-viscoelasticity half space using different theories. The propagation of plane harmonic waves in a rotating elastic medium without the thermal field has been studied. It was shown that the rotation causes the elastic medium to be dispersive and isotropic. Those problems are based on more realistic elastic models, since the Earth and its moon, and other planets all have angular velocities.

Othman and Song[21] showed the effect of the initial stress, thermoelastic parameter, and thermal boundary condition on the reflection amplitude ratios. The problem of magneto-elastic transverse surface waves in the self-reinforced elastic solid was studied by Verma *et al.*[22] The problem of wave propagation in thermally conducting linear fibre-reinforced composite materials was discussed by Singh.[23]

Othman and Lotfy[24] studied the two-dimensional problem of generalized magneto-thermoelasticity under the effect of temperature dependent properties. Othman and Lotfy[25] studied transient disturbance in a half-space under the generalized magneto-thermoelasticity with moving internal heat sources. Othman and Lotfy[26] studied the plane waves in a generalized thermo-microstretch elastic half-space by using a general model of equations of generalized thermo-microstretch for a homogeneous isotropic elastic half space. Othman and Lotfy[27] studied the generalized thermo-microstretch elastic medium with temperature dependent properties using different theories. Othman and Lotfy[28] studied the effect of magnetic field and inclined load in micropolar thermoelastic medium possessing cubic symmetry under three theories. The normal mode analysis was used to obtain the exact expression for the temperature distribution, thermal stresses, and the displacement components.

In recent years, considerable efforts have been devoted to the study of failure and cracks in solids. This is due to the application of the latter in industry and particularly in the fabrication of electronic components. Most of the studies of the dynamical crack problem are done using the equations of coupled or even uncoupled theories of thermoelasticity,[29−32] which is suitable for most situations where long time effects are sought. However, when the short time behaviours are important, as in many practical situations, the full system of the generalized thermoelastic equations must be used.[13]

In the present work, we shall formulate the fibre-reinforced two-dimensional problem of thermoelasticity for an infinite space weakened by a finite linear opening mode-I crack. The normal mode method is used to obtain the exact expressions for the considering variables. The distributions of the considering variables are represented graphically. A comparison is carried out between the generalized thermo-elasticity L–S and the coupled theories for the temperature, the stresses, and the displacements in the half space fibre-reinforced problem. A comparison is also made between the two theories for different depths.

2. Formulation of the problem and basic equations

The constitutive equations for a fibre-reinforced linearly elastic anisotropic medium with respect to the reinforcement direction $\boldsymbol{a}$ are (Belfied *et al.*[1])

$$\begin{aligned}\sigma_{ij} =& \lambda e_{kk}\delta_{ij} + 2\mu_{\mathrm{T}} e_{ij} + \alpha(a_k a_m e_{km}\delta_{ij} + a_i a_j e_{kk}) \\ &+ 2(\mu_{\mathrm{L}} - \mu_{\mathrm{T}})(a_i a_k e_{kj} + a_j a_k e_{ki}) \\ &+ \beta a_k a_m e_{km} a_i a_j \\ &- \gamma\Big(1 + \nu_0 \frac{\partial}{\partial t}\Big)(T - T_0)\delta_{ij}, \end{aligned} \tag{1}$$

where σ_{ij} are the components of stress; e_{ij} are the components of strain; $\lambda, \mu_{\mathrm{T}}$ are the elastic constants; $\alpha, \beta, (\mu_{\mathrm{L}} - \mu_{\mathrm{T}})$ are the reinforcement parameters; $\gamma = (3\lambda + 2\mu)\alpha_{\mathrm{t}}$, α_{t} is the thermal expansion coefficient; and $\boldsymbol{a} \equiv (a_1, a_2, a_3)$, with $a_1^2 + a_2^2 + a_3^2 = 1$. We choose the fibre direction as $\boldsymbol{a} \equiv (1, 0, 0)$. The strains can be expressed in terms of displacement u_i as

$$e_{ij} = \frac{1}{2}(u_{i,j} + u_{j,i}). \tag{2}$$

For the plane strain deformation in the xy plane (displacement $u = (u, v, 0)$), $\frac{\partial}{\partial z} = 0$, $w = 0$. Equation (1) then yields

$$\sigma_{xx} = A_{11}u_{,x} + A_{12}v_{,y} - \gamma\Big(1 + \nu_0\frac{\partial}{\partial t}\Big)(T - T_0), \tag{3}$$

$$\sigma_{yy} = A_{22}v_{,y} + A_{12}u_{,x} - \gamma\Big(1 + \nu_0\frac{\partial}{\partial t}\Big)(T - T_0), \tag{4}$$

$$\sigma_{zz} = A_{12}u_{,x} + \lambda v_{,y} - \gamma\Big(1 + \nu_0\frac{\partial}{\partial t}\Big)(T - T_0), \tag{5}$$

$$\sigma_{xy} = \mu_{\mathrm{L}}(u_{,y} + v_{,x}), \quad \sigma_{zx} = \sigma_{zy} = 0, \tag{6}$$

where

$$\begin{aligned} &A_{11} = \lambda + 2(\alpha + \mu_{\mathrm{T}}) + 4(\mu_{\mathrm{L}} - \mu_{\mathrm{T}}) + \beta, \\ &A_{12} = \alpha + \lambda, \quad A_{22} = \lambda + 2\mu_{\mathrm{T}}. \end{aligned} \tag{7}$$

Since the medium is rotating uniformly with an angular velocity $\boldsymbol{\Omega} = \Omega\boldsymbol{n}$ (Fig. 1), where $\boldsymbol{n}$ is a unit vector representing the direction of the axis of rotation, the displacement equation of motion in the rotating reference frame has two additional terms, the centripetal acceleration $\boldsymbol{\Omega}x$ $(\boldsymbol{\Omega}x\boldsymbol{u})$ due to the time-varying motion only and the Corioli's acceleration $2\boldsymbol{\Omega}x\dot{\boldsymbol{u}}$, where $\boldsymbol{u}$ is the dynamic displacement vector.

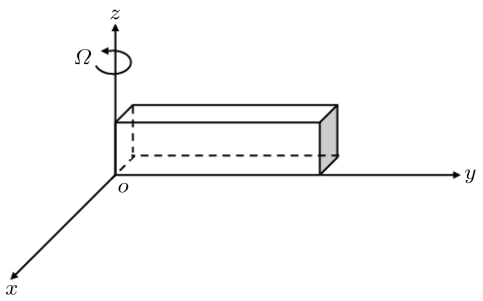


Fig. 1. Geometry of the problem.

The equations of motion in the rotating reference frame in the context of generalized thermo elasticity are

$$\begin{aligned}&\rho[\ddot{u}_i + \{\boldsymbol{\Omega}x(\boldsymbol{\Omega}x\boldsymbol{u})\}_i + (2\boldsymbol{\Omega}x\dot{\boldsymbol{u}})_i] = \sigma_{ij,j}, \\ &\qquad (i, j = 1, 2, 3). \end{aligned} \tag{8}$$

The heat conduction equation is

$$\begin{aligned} kT_{,ii} =& \Big(n_1\frac{\partial}{\partial t} + \tau_0\frac{\partial^2}{\partial t^2}\Big)\rho C_{\mathrm{E}}T \\ &+ \gamma T_0\Big(n_1\frac{\partial}{\partial t} + n_0\tau_0\frac{\partial^2}{\partial t^2}\Big)u_{i,i}, \end{aligned} \tag{9}$$

where ρ is the density, k is the thermal conductivity, C_{E} is the specific heat at a constant strain, and T is the temperature above reference temperature T_0.

Using the summation convection, from Eqs. (3)–(6), we note that the third equation of motion in Eq. (8) identically satisfies and the first two equations become

$$\begin{aligned}&\rho\Big(\frac{\partial^2 u}{\partial t^2} - \Omega^2 u - 2\Omega\dot{v}\Big) \\ &= A_{11}\frac{\partial^2 u}{\partial x^2} + B_2\frac{\partial^2 v}{\partial x\partial y} + B_1\frac{\partial^2 u}{\partial y^2} - \gamma\Big(1 + \nu_0\frac{\partial}{\partial t}\Big)\frac{\partial T}{\partial x}, \end{aligned} \tag{10}$$

$$\begin{aligned}&\rho\Big(\frac{\partial^2 v}{\partial t^2} - \Omega^2 v + 2\Omega\dot{u}\Big) \\ &= A_{22}\frac{\partial^2 v}{\partial y^2} + B_2\frac{\partial^2 u}{\partial x\partial y} + B_1\frac{\partial^2 v}{\partial x^2} - \gamma\Big(1 + \nu_0\frac{\partial}{\partial t}\Big)\frac{\partial T}{\partial y}, \end{aligned} \tag{11}$$

where $B_1 = \mu_{\mathrm{L}}$, $B_2 = \alpha + \lambda + \mu_{\mathrm{L}}$.

Equations (3)–(6) and (9)–(11) are the field equations of the generalized thermoelasticity elastic solid applicable to the L–S, the G–L, and the classical coupled (CD) theories, as they become the equations of i) the coupled thermo-elasticity theory, when $n_0 = 0$, $n_1 = 1$, $\tau_0 = \nu_0 = 0$; ii) the L–S theory, when $n_1 = n_0 = 1$, $\nu_0 = 0$, $\tau_0 > 0$; iii) the G–L theory, when $n_1 = 1$, $n_0 = 0$, $\nu_0 \geq$, $\tau_0 > 0$. Neglecting the angular velocity (i.e. $\Omega = 0$) in Eqs. (10) and (11), we obtain the transformed components of displacement, stress forces, and temperature distribution in a non-rotating generalized thermoelasticity medium.

For convenience, the following non-dimensional variables are used:

$$\begin{aligned}&x' = c_1\eta x,\ y' = c_1\eta\, y,\ u' = c_1\eta\, u,\ v' = c_1\eta\, v, \\ &t' = c_1^2\eta\, t,\ \tau_0' = c_1^2\eta\,\tau_0,\ \Omega' = \frac{\Omega}{c_1^2\eta},\ \nu_0' = c_1^2\eta\,\nu_0, \\ &\theta = \gamma\frac{(T - T_0)}{\lambda + 2\mu_{\mathrm{T}}},\ \sigma_{ij}' = \frac{\sigma_{ij}}{\mu_{\mathrm{T}}},\ i, j = 1, 2, \end{aligned} \tag{12}$$

where $\eta = \dfrac{\rho\, C_{\mathrm{E}}}{k}$, $c_1^2 = \dfrac{\lambda + 2\mu_{\mathrm{T}}}{\rho}$.

In terms of the non-dimensional quantities defined in Eq. (12), the above governing equations reduce to (dropping the dash for convenience)

$$\frac{\partial^2 u}{\partial t^2} - \Omega^2 u - 2\Omega\dot{v} = h_{11}\frac{\partial^2 u}{\partial x^2} + h_2\frac{\partial^2 v}{\partial x \partial y} + h_1\frac{\partial^2 u}{\partial y^2} - \Big(1 + \nu_0\frac{\partial}{\partial t}\Big)\frac{\partial \theta}{\partial x}, \tag{13}$$

$$\frac{\partial^2 v}{\partial t^2} - \Omega^2 v + 2\Omega\dot{u} = h_{22}\frac{\partial^2 v}{\partial y^2} + h_2\frac{\partial^2 u}{\partial x \partial y} + h_1\frac{\partial^2 v}{\partial x^2} - \Big(1 + \nu_0\frac{\partial}{\partial t}\Big)\frac{\partial \theta}{\partial y}, \tag{14}$$

$$\frac{\partial^2 \theta}{\partial x^2} + \frac{\partial^2 \theta}{\partial y^2} = \Big(n_1\frac{\partial}{\partial t} + \tau_0\frac{\partial^2}{\partial t^2}\Big)\theta + \varepsilon\Big(n_1\frac{\partial}{\partial t} + n_0\tau_0\frac{\partial^2}{\partial t^2}\Big)\Big(\frac{\partial u}{\partial x} + \frac{\partial v}{\partial y}\Big), \tag{15}$$

where

$$(h_{11}, h_{22}, h_1, h_2) = \frac{(A_{11}, A_{22}, B_1, B_2)}{(\lambda + 2\mu_{\rm T})},$$

$$\varepsilon = \frac{\gamma^2 T_0}{\rho C_{\rm E}(\lambda + 2\mu_{\rm T})},$$

$$\mu_{\rm T}\sigma_{xx} = A_{11}u_{,x} + A_{12}v_{,y} - A_{22}\Big(1 + \nu_0\frac{\partial}{\partial t}\Big)\theta, \tag{16}$$

$$\mu_{\rm T}\sigma_{yy} = A_{22}v_{,y} + A_{12}u_{,x} - A_{22}\Big(1 + \nu_0\frac{\partial}{\partial t}\Big)\theta, \tag{17}$$

$$\mu_{\rm T}\sigma_{zz} = A_{12}u_{,x} + \lambda v_{,y} - A_{22}\Big(1 + \nu_0\frac{\partial}{\partial t}\Big)\theta, \tag{18}$$

$$\mu_{\rm T}\sigma_{xy} = \mu_{\rm L}\Big(u_{,y} + v_{,x}\Big),\ \sigma_{zx} = \sigma_{zy} = 0. \tag{19}$$

3. Normal mode analysis

The normal mode analysis gives exact solutions without any assumed restrictions on temperature, displacement, and stress distributions. It is applied to a wide range of problems in different branches (Othman,[33] Ezzat *et al.* [34,35] Othman and Singh,[36] Othman and Kumar[37]). It can be applied to boundary-layer problems, which are described by the linearized Navier–Stokes equations in electro hydrodynamics. The normal mode analysis is, in fact, to look for the solution in the Fourier transformed domain, assuming that all the field quantities are sufficiently smooth on the real line so that the normal mode analysis of these functions exists. The solution of the considered physical variable can be decomposed in terms of normal modes as

$$\begin{aligned}&[u, v, \theta, \sigma_{ij}](x, y, t)\\ &= [u^*(x), v^*(x), \theta^*(x), \sigma^*_{ij}(x)]\exp(\omega t + {\rm i}\, ay),\end{aligned} \tag{20}$$

where ω is the (complex) time constant, ${\rm i} = \sqrt{-1}$, a is the wave number in the y direction, and $u^*(x)$, $v^*(x)$, $\theta^*(x)$, and $\sigma^*_{ij}(x)$ are the amplitudes of the field quantities. Using Eq. (20), Eqs. (13)–(19) take the form

$$(h_{11}D^2 - A_1)\,u^* + (2\Omega\omega + {\rm i}\, ah_2 D)v^* = QD\theta^*, \tag{21}$$

$$(h_1 D^2 - A_2)\,v^* + (-2\Omega\omega + {\rm i}\, ah_2 D)\,u^* = {\rm i}\, aQ\theta^*, \tag{22}$$

$$A_4 D\,u^* + {\rm i}\, aA_4 v^* = (D^2 - A_3)\theta^*, \tag{23}$$

$$\mu_{\rm T}\sigma^*_{xx} = A_{11}D\,u^* + {\rm i}\, aA_{12}v^* - A_{22}Q\theta^*, \tag{24}$$

$$\mu_{\rm T}\sigma^*_{yy} = A_{12}D\,u^* + {\rm i}\, aA_{22}v^* - A_{22}Q\theta^*, \tag{25}$$

$$\mu_{\rm T}\sigma^*_{zz} = A_{12}D\,u^* + {\rm i}\, a\lambda\, v^* - A_{22}Q\theta^*, \tag{26}$$

$$\mu_{\rm T}\sigma^*_{xy} = \mu_{\rm L}({\rm i}\, a\,u^* + D\,v^*),\ \sigma^*_{zx} = \sigma^*_{zy} = 0, \tag{27}$$

where

$$\begin{aligned}&A_1 = \omega^2 - \Omega^2 + h_1 a^2,\ A_2 = \omega^2 - \Omega^2 + h_{22}a^2,\\ &Q = 1 + \omega\nu_0, \qquad\qquad A_3 = a^2 + \omega(n_1 + \omega\tau_0),\\ &A_4 = \omega\varepsilon(n_1 + n_0\omega\tau_0),\quad D = \frac{\rm d}{{\rm d}x}.\end{aligned}$$

Eliminating $\theta^*(x)$ and $v^*(x)$ in Eqs. (21)–(23), we obtain the partial differential equation satisfied by $u^*(x)$

$$(D^6 - AD^4 + B\,D^2 - C)\,u^*(x) = 0, \tag{28}$$

where

$$\begin{aligned}A = &\frac{1}{h_1 h_{11}}(h_{11}A_2 + h_1 A_1 + h_1 A_4 Q\\ &+ h_1 h_{11}A_3 - h_2^2 a^2),\end{aligned} \tag{29}$$

$$\begin{aligned}B = &\frac{1}{h_1 h_{11}}\big[A_1 A_2 + h_{11}A_2 A_3 + h_1 A_1 A_3\\ &+ Q(h_{11}a^2 A_4 + A_2 A_4 - 2h_2 a^2 A_4)\\ &+ 4\Omega^2\omega^2 - h_2^2 a^2 A_3\big],\end{aligned} \tag{30}$$

$$C = \frac{1}{h_1 h_{11}}(A_1 A_2 A_3 + A_1 A_4 a^2 Q + 4\Omega^2\omega^2 A_3). \tag{31}$$

In a similar manner, we get

$$\big(D^6 - AD^4 + BD^2 - C\big)\{v^*(x), \theta^*(x)\} = 0. \tag{32}$$

The above equation can be factorized as

$$(D^2 - k_1^2)(D^2 - k_2^2)(D^2 - k_3^2)u^*(x) = 0, \tag{33}$$

where k_n^2 $(n = 1, 2, 3)$ are the roots of the following characteristic equation

$$k^6 - Ak^4 + Bk^2 - C = 0. \tag{34}$$

The solution of Eq. (33), which is bounded at $x \to \infty$, is given by

$$u^*(x) = \sum_{n=1}^{3} M_n(a, \omega)\exp(-k_n x). \tag{35}$$

Similarly

$$v^*(x) = \sum_{n=1}^{3} M'_n(a, \omega)\exp(-k_n x), \tag{36}$$

$$\theta^*(x) = \sum_{n=1}^{3} M''_n(a, \omega)\exp(-k_n x), \tag{37}$$

where M_n, M'_n, and M''_n are some parameters depending on a and ω. Substituting Eqs. (35)–(37) into Eqs. (21)–(23), we have ($n = 1, 2, 3$)

$$M'_n(a,\omega) = H_{1n} M_n(a,\omega), \tag{38}$$

$$M''_n(a,\omega) = H_{2n} M_n(a,\omega), \tag{39}$$

where

$$H_{1n} = \frac{-\mathrm{i}\, a h_{11} k_n^2 + \mathrm{i}\, a A_1 + 2\Omega\omega\, k_n + \mathrm{i}\, a h_2 k_n^2}{2\,\mathrm{i}\, a\Omega\omega + h_2 k_n a^2 + h_1 k_n^3 - A_2 k_n}, \tag{40}$$

$$H_{2n} = \frac{-A_4\, k_n + \mathrm{i}\, a A_4 H_{1n}}{k_n^2 - A_3}. \tag{41}$$

Thus, we have

$$v^*(x) = \sum_{n=1}^{3} H_{1n}\, M_n(a,\omega) \exp(-k_n x), \tag{42}$$

$$\theta^*(x) = \sum_{n=1}^{3} H_{2n} M_n(a,\omega) \exp(-k_n x). \tag{43}$$

Substituting Eqs. (35), (42), and (43) into Eqs. (24)–(27), we obtain

$$\sigma^*_{xx} = \sum_{n=1}^{3} H_{3n}\, M_n(a,\omega)\, \exp(-k_n x), \tag{44}$$

$$\sigma^*_{yy} = \sum_{n=1}^{3} H_{4n}\, M_n(a,\omega)\, \exp(-k_n x), \tag{45}$$

$$\sigma^*_{zz} = \sum_{n=1}^{3} H_{5n}\, M_n(a,\omega)\, \exp(-k_n x), \tag{46}$$

$$\sigma^*_{xy} = \sum_{n=1}^{3} H_{6n}\, M_n(a,\omega)\, \exp(-k_n x), \tag{47}$$

where

$$H_{3n} = (-A_{11} k_n + \mathrm{i}\, a A_{12} H_{1n} - A_{22} Q H_{2n})/\mu_{\mathrm{T}}, \tag{48}$$

$$H_{4n} = (-A_{12} k_n + \mathrm{i}\, a A_{22} H_{1n} - A_{22} Q H_{2n})/\mu_{\mathrm{T}}, \tag{49}$$

$$H_{6n} = \mu_{\mathrm{L}}(\mathrm{i}\, a - k_n H_{1n})/\mu_{\mathrm{T}}, \tag{50}$$

$$H_{5n} = (-A_{12} k_n + \mathrm{i}\, a\lambda H_{1n} - A_{22} Q H_{2n})/\mu_{\mathrm{T}}. \tag{51}$$

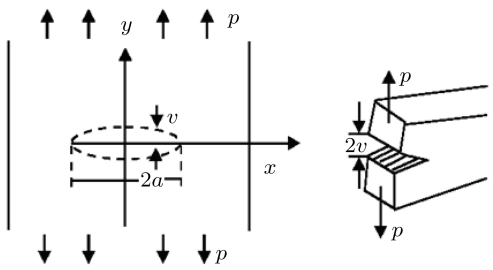


Fig. 2. Displacement of an external mode-I crack.

We now apply above analysis to model-I crack as shown in Fig. 2. The plane boundary subjects to an instantaneous normal point force, and the boundary surface is isothermal, the boundary conditions at the vertical plan $y = 0$ and in the beginning of the crack at $x = 0$ are

$$\sigma_{yy}(x,y,t) = -p(0,y,t), \tag{52}$$

$$\theta(x,y,t) = f(0,y,t), \quad \frac{\partial\theta}{\partial y} = 0, \tag{53}$$

$$\sigma_{xy}(x,y,t) = 0. \tag{54}$$

Substituting the expressions of the variables considered into the above boundary conditions, we obtain

$$\sum_{n=1}^{3} H_{3n} M_n(a,\omega) = -p, \tag{55}$$

$$\sum_{n=1}^{3} H_{2n} M_n(a,\omega) = f, \tag{56}$$

$$\sum_{n=1}^{3} H_{6n} M_n(a,\omega) = 0. \tag{57}$$

Invoking boundary conditions (55)–(57) at surface $x = 0$ of the plate, we obtain a system of three equations. After applying the inverse of matrix method, we have the values of the three constants $M_j (j = 1, 2, 3)$

$$\begin{pmatrix} M_1 \\ M_2 \\ M_3 \end{pmatrix} = \begin{pmatrix} H_{41} & H_{42} & H_{43} \\ H_{21} & H_{22} & H_{23} \\ H_{61} & H_{62} & H_{63} \end{pmatrix}^{-1} \begin{pmatrix} -p^* \\ f^* \\ 0 \end{pmatrix}.$$

Hence, we obtain the expressions for the displacements, the temperature distribution, and another physical quantities of the plate muscles.

4. Numerical results

With the analytical procedure presented earlier, we now consider a numerical example, for which computational results are given. The results depict the variations of temperature, displacement, and stress fields in the context of the three theories. To study the effects of rotation and reinforcement on the wave propagation, we use the following physical constants:

$$\lambda = 7.59 \times 10^9\ \mathrm{N/m^2}, \quad \mu_{\mathrm{T}} = 1.89 \times 10^9\ \mathrm{N/m^2},$$
$$\mu_{\mathrm{L}} = 2.45 \times 10^9\ \mathrm{N/m^2}, \quad \alpha = -1.28 \times 10^9\ \mathrm{N/m^2},$$
$$\beta = 0.32 \times 10^9\ \mathrm{N/m^2}, \quad \rho = 7800\ \mathrm{kg/m^2},$$
$$\alpha_{\mathrm{t}} = 1.78 \times 10^{-5}\ \mathrm{N/m^2}, \quad k = 386, \quad C_{\mathrm{E}} = 383.1,$$
$$\tau_0 = 0.02, \quad a = 1, \quad T_0 = 293\ \mathrm{K}, \quad f^* = 1,$$
$$p^* = 2, \quad \omega = \omega_0 + \mathrm{i}\,\xi, \quad \omega_0 = 2, \quad \xi = 1,$$
$$C_{\mathrm{E}} = 383.1\ \mathrm{J/(kg \cdot K)}, \quad \mu = 3.86 \times 10^{10}\ \mathrm{kg/ms^2}.$$

The calculations are carried out for a time of $t = 0.1$. The numerical technique outlined above is used for the distribution of the real part of the thermal temperature θ, the displacements u and v, the distributions of stresses σ_{xx}, σ_{yy}, σ_{zz}, and σ_{xy} for the problem. The

field quantities including temperature, displacement components u, v, and stress components σ_{xx}, σ_{yy}, σ_{zz}, and σ_{xy} depend not only on space x and time t, but also on thermal relaxation time τ_0 and ν_0. Here all the variables are taken in the non-dimensional forms. Two different values of Ω ($\Omega = 0$ and $\Omega = 0.2$ i.e., in the absence and the presence of the rotation) are considered.

The results are shown in Figs. 3–9. The graphs show the three results predicted by the different theories of thermoelasticity. In these figures, the solid lines represent the solution of the coupled theory, the dotted lines represent the solution of the generalized Lord and Şhulman theory, and the dashed lines represent the solution derived using the Green and Lindsay theory. We notice that the results for the temperature, the displacement, and stress distributions with the relaxation time included in the heat equation are distinctly different from those without the relaxation time in the heat equation, because the thermal wave in the Fourier theory of heat travel has an infinite speed of propagation as opposed to the finite speed in the non-Fourier case. This demonstrates clearly the difference between the coupled theory and the theory of thermoelasticity (L–S theory).

The value of y, namely $y = 1$, is substituted in performing the computation. It should be noted (Fig. 3) that in this problem, the crack size x is taken to be the length, so $0 \leq x \leq 2$. The $y = 0$ represents the plane of the crack, which is symmetric with respect to the y plane. It is clear from the graph that θ obtains the maximum value at the beginning of the crack, and it begins to fall just near the crack edge ($x \approx 1.1$), where it experiences smooth decreases (with the maximum negative gradient at the crack end). The value of temperature quantity converges to zero with the increase of distance x. The effect of rotation on temperature decreases the value of the amplitude of θ.

As shown in Fig. 4, horizontal displacement u increases near the crack edge (always starts from a negative value and terminates at the zero value), then smooth decreases again to reach its minimum magnitude just at about the crack end. Beyond the end, u falls again to retain zero at infinity. The values of u for $\Omega = 0.2$ are smaller compared to those for $\Omega = 0.0$. The behaviours of displacement u in the CD, the L–S, and the G–L theories for the two different values of rotation are similar.

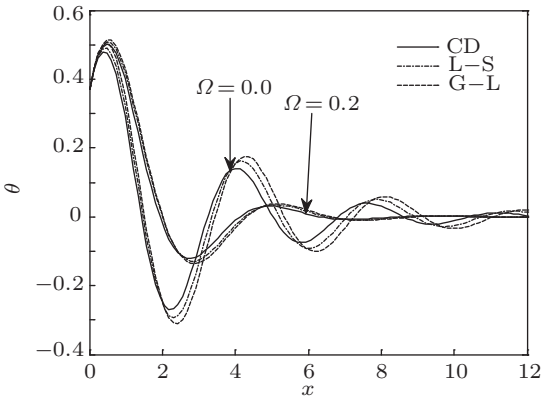


Fig. 3. Temperature distribution θ at different rotation speeds.

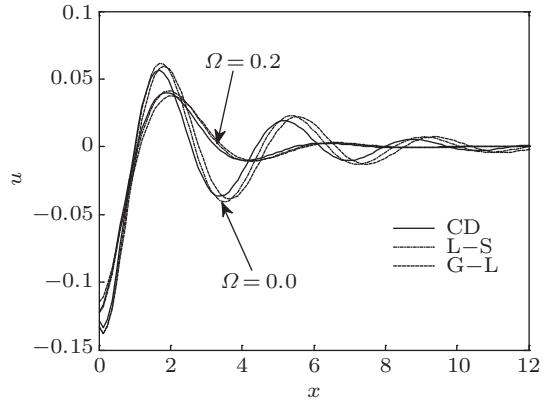


Fig. 4. Horizontal displacement distribution u at different rotation speeds.

Figure 5 shows vertical displacement v. We can see that displacement component v always starts from a negative value and terminates at the zero value when $\Omega = 0.2$. Also, at the crack end, it reaches the maximum value. It reaches zero at the three double of the crack size (state of particle equilibrium). When $\Omega = 0.0$, displacement component v always starts from a positive value, reaches the minimum value at the crack end, and is zero at the three double of the crack size (state of particle equilibrium).

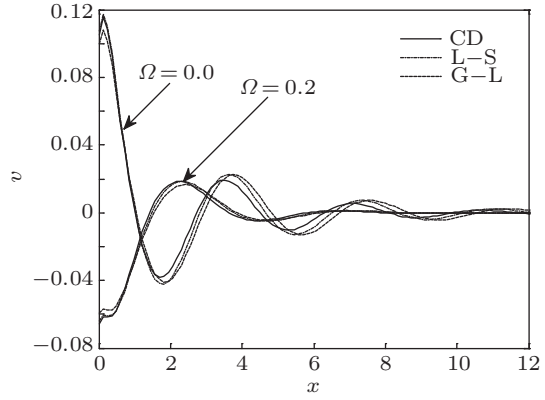


Fig. 5. Vertical displacement distribution v at different rotation speeds.

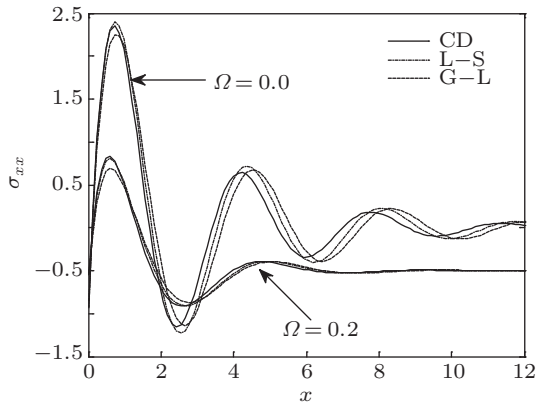


Fig. 6. Distributions of stress component σ_{xx} at different rotation speeds.

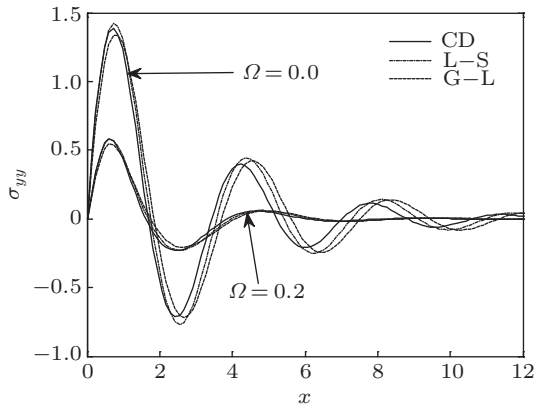


Fig. 7. Distributions of stress component σ_{yy} at different rotation speeds.

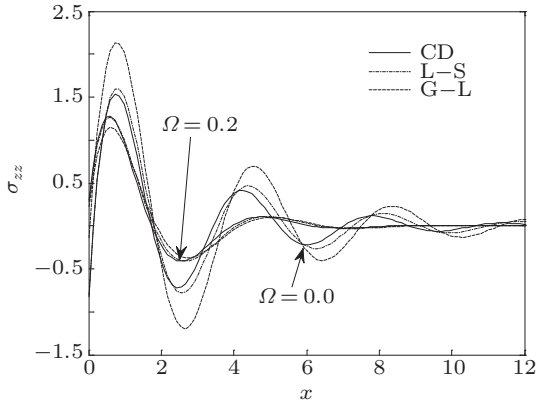


Fig. 8. Distributions of stress component σ_{zz} at different rotation speeds.

Displacements u and v show different behaviours, because the elasticity of the solid tends to resist vertical displacements in the problem under investigation. Both of the components show different behaviours, the former tends to increase to the maximum just before the end of the crack. Then it falls to the minimum with a highly negative gradient. Afterwards, it rises again to the maximum beyond the crack end.

The stress component σ_{xx} reaches coincidence with a negative value (Fig. 6) and satisfies the boundary condition at $x = 0$. It reaches the minimum value near the end of the crack and converges to zero with the increasing distance x. The behaviours of the two cases with different values of rotation are similar. The rotation decreases the amplitudes of the stress. Figures 7 and 8 show the same behaviour as that found in Fig. 6.

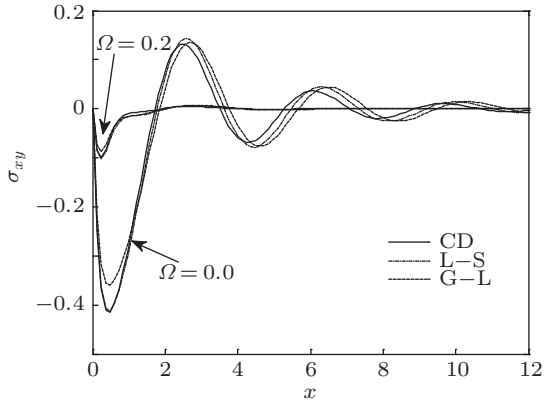


Fig. 9. Distributions of stress component σ_{xy} at different rotation speeds.

Figure 7 shows that stress component σ_{xy} satisfies the boundary condition at $x = 0$ and has a different behaviour compared to that of σ_{xx}. It decreases at the beginning and starts to increase (maximum) in the context of the three theories until reaching the crack end for $\Omega = 0.2$. When $\Omega = 0.0$, it decreases at the beginning and starts to increase (maximum) in the context of the three theories until reaching the crack end. These trends obey elastic and thermoelastic properties of the solid under investigation.

Figures 10–16 show temperature θ, displacement components u, v, force stress components σ_{xx}, $\sigma_{yy}\sigma_{zz}$, and σ_{xz} for three different values of y (namely, $y = 1$, $y = 1.2$, and $y = 1.4$) and two different values of rotation under the G–L theory.

It is clear from the graph that θ increases to the maximum value at the beginning of the crack ($x = 0$). It begins to fall just near the crack edge ($x \approx 1.2$), where it experiences smooth decreases (with the minimum negative gradient at the crack end). The lines for different values of y show different slopes at the crack ends. More specifically, the temperature line for $y = 1$ has the highest gradient compared with that for $y = 1.2$ and $y = 1.4$ at the first range. In addition, all lines begin to coincide to reach the reference temperature of the solid when the horizontal distance x is beyond the three doubles of the crack size. These results obey the physical reality for the behaviour of the fibre as a polycrystalline solid.

Figure 11 shows horizontal displacement u. Despite the peaks (for different vertical distances $y = 1$, $y = 1.2$, and $y = 1.4$) occur at the equal value of x, the magnitudes of the maximum displacement strongly depend on vertical distance y. It is also clear that the rate of change of u decreases with the increasing y as we go further away from the crack. On the other hand, Fig. 12 shows the atonable increase of vertical displacement v. It reaches the minimum value near the crack end, and reaches zero at the three doubles of the crack size (state of particle equilibrium).

Figure 13 shows horizontal stresses σ_{xx}. The lines for different values of y show different slopes at the crack ends. In other words, the σ_{xx} component line for $y = 1.4$ has the highest gradient compared with that for $y = 1.2$ and $y = 1$ at the edge of the crack when $\Omega = 0.2$. In addition, all lines begin to coincide to reach zero after their relaxations at infinity when horizontal distance x is beyond the three doubles of the crack size. The variation of y has a serious effect on all magnitudes of mechanical stresses. These trends obey the elastic and thermoelastic properties of the solid under investigation.

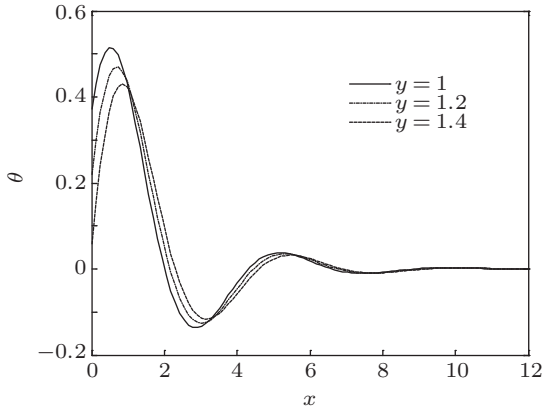


Fig. 10. Temperature distribution θ obtained with the G–L theory.

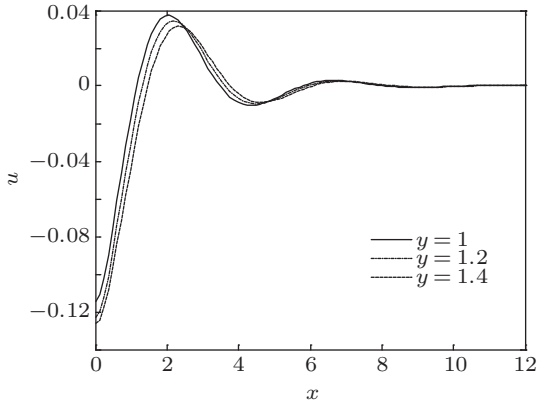


Fig. 11. Displacement distribution u obtained with the G–L theory.

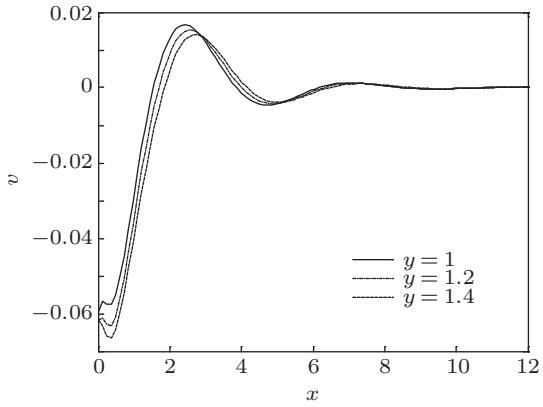


Fig. 12. Displacement distribution v obtained with the G–L theory.

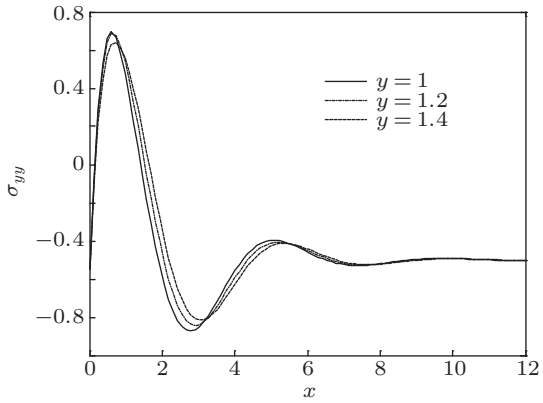


Fig. 13. Stress distribution σ_{xx} obtained with the G–L theory.

Figure 14 shows stress component σ_{yy}. The line for $y = 1.4$ has the highest gradient compared with that for $y = 1.2$ and $y = 1$ in the range of $1.2 \leq x \leq 2.4$ (near the crack edge). The line for $y = 1$ has the highest gradient compared with that for $y = 1.2$ and $y = 1.4$ in the range of $2.4 \leq x \leq 5$ (near the crack end) and converges to zero when $x > 10$. These trends obey elastic and thermoelastic properties of the solid, which is also true for Fig. 15.

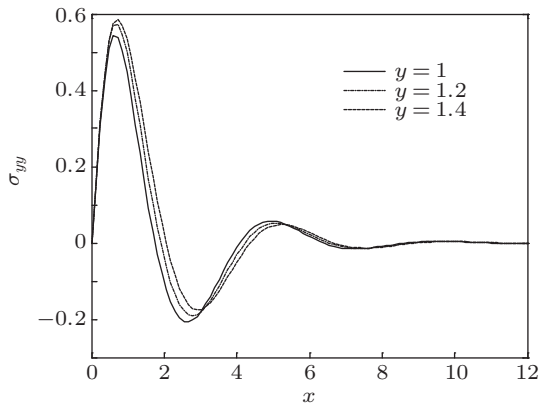


Fig. 14. Stress distribution σ_{yy} obtained with the G–L theory.

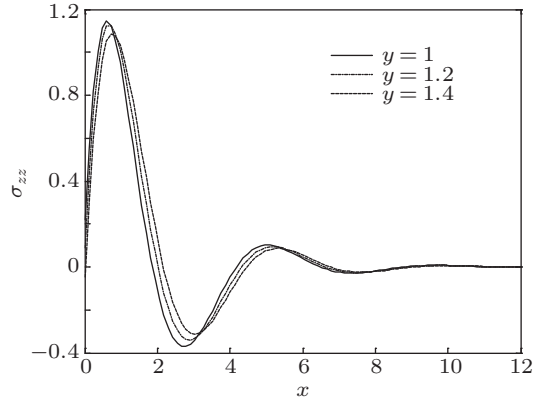


Fig. 15. Stress distribution σ_{zz} obtained with the G–L theory.

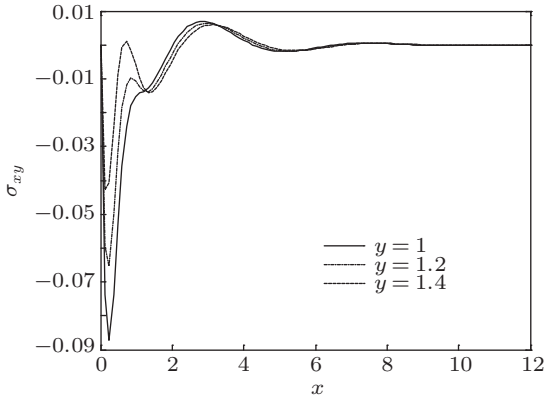


Fig. 16. Stress distribution σ_{xy} obtained with the G–L theory.

Figure 14 shows that stress component σ_{xy} satisfies the boundary condition. It sharply decreases at the beginning and starts to increase (minimum) in the context of the three values of y until reaching the crack end. The line for $y = 1.4$ has the highest gradient compared with that for $y = 1.2$ and $y = 1$ in the range of $0 \leq x \leq 2$. The line for $y = 1$ has the highest gradient compared with that for $y = 1.2$ and $y = 1.4$ in the range of $2 \leq x \leq 3.5$ and converges to zero when $x > 8$. These trends obey elastic and thermoelastic properties of the solid.

5. Conclusion

Analytical solutions based on the normal mode analysis for the themoelastic problem in solids have been developed and utilized. A linear opening mode-I crack has been investigated and studied for the copper solid. Temperature, radial, and axial distributions are estimated at different distances from the crack edge. The stress distributions and the temperature are evaluated as functions of the distance from the crack edge. We find that the curves in the context of the CD, the L–S, and the G–L theories decrease exponentially with the increasing x, which indicates that the thermoelastic waves are unattenuated and nondispersive, while purely thermoelastic waves undergo both attenuation and dispersion. The curves of the physical quantities obtained with the CD theory in most of the figures are lower in comparison with those obtained with the L–S and the G–L theories, which is due to the relaxation time. The values of all the physical quantities converge to zero with an increase in distance y, and all functions are continuous. The fibre-reinforcement has an important role on the distributions of the field quantities. The presence of rotation plays a significant role in all the physical quantities. The amplitudes of all the physical quantities decrease when the rotation speed increases. Therefore, the presence of rotation in the current model is of significance. Crack dimensions are significant to elucidate the mechanical structure of the solid. Cracks are stationary, and the external stress is demanded to propagate such cracks. It can be concluded that a change of volume is attended by a change of the temperature, while the effect of the deformation on the temperature distribution is the subject of the theory of thermoelasticity. The method, which is used in the present article, is applicable to a wide range of problems in thermodynamics and thermoelasticity.

References

[1] Belfield A J, Rogers T G and Spencer A J M 1983 *J. Mech. Phys. Solids* **31** 25
[2] Verma P D S and Rana O H 1983 *Mech. Materials* **2** 353
[3] Verma P D S 1986 *Int. J. Eng. Sci.* **24** 1067
[4] Singh S J 2002 *Sãdhanã* **27** 1
[5] Sengupta P R and Nath S 2001 *Sãdhanã* **26** 363
[6] Hashin Z and Rosen W B 1964 *J. Appl. Mech.* **31** 223
[7] Singh B and Singh S J 2004 *Sãdhanã* **29** 249
[8] Chattopadhyay A and Choudhury S 1990 *Int. J. Eng. Sci.* **28** 485
[9] Chaudhary S, Kaushik V P and Tomar S K 2004 *Acta Geoph. Polonica* **52** 219
[10] Chattopadhyay A and Choudhury S 1995 *Int. J. Num. Anal. Meth. Geomech.* **19** 289
[11] Pradhan A S, Samal K and Mahanti N C 2003 *Tamkang J. Sci. Eng.* **6:3** 173
[12] Chattopadhyay A, Venkateswarlu R L K and Saha S 2002 *Sãdhanã* **27** 613
[13] Lord H W and Şulman Y A 1967 *J. Mech. Phys. Solid* **15** 299
[14] Green A E and Lindsay K A 1972 *J. Elasticity* **2** 1
[15] Roy Choudhuri S K and Debnath L 1983 *Int. J. Eng. Sci.* **21** 155
[16] Roy Choudhuri S K and Debnath L 1983 *J. Appl. Mech.* **50** 283
[17] Othman M I A 2005b *Int. J. Solids Struct.* **41** 2939
[18] Othman M I A 2005 *Acta Mechanica* **174** 129

[19] Othman M I A and Singh B 2007 *Int. J. Solids Stru.* **44** 2748

[20] Othman M I A and Song Y 2008 *Appl. Math. Modelling* **32** 811

[21] Othman M I A and Song Y 2007 *Int. J. Sol. Stru.* **44** 5651

[22] Verma P D S, Rana O H and Verma M 1988 *Indian J. Pure Appl. Math.* **19** 713

[23] Singh B 2006 *Arch. Appl. Mech.* **75** 513

[24] Othman M I A and Lotfy KH 2009 *MMMS* **5** 235

[25] Othman M I A, Lotfy KH and Farouk R M 2009 *Acta Physica Polonica* A **116** 186

[26] Othman M I A and Lotfy KH 2010 *Int. Commun. in Heat and Mass Transfer* **37** 192

[27] Othman M I A and Lotfy KH 2009 *Int. J. of Ind. Math.* **2** 87

[28] Othman M I A and Lotfy KH 2010 *Eng. Anal. with Boundary Elements* **34** 229

[29] Dhaliwal R 1980 *External Crack due to Thermal Effects in an Infinite Elastic Solid with a Cylindrical Inclusion. Thermal Stresses in Server Environments* (New York: Plenum Press) pp. 665–692

[30] Hasanyan D, Librescu L, Qin Z and Young R 2005 *J. Thermal Stresses* **28** 729

[31] Ueda S 2003 *J. Thermal Stresses* **26** 311

[32] Elfalaky A and Abdel-Halim A A 2006 *J. Applied Sciences* **6** 598

[33] Othman M I A 2002 *J. Thermal stresses* **25** 1027

[34] Ezzat M, Othman M I A and El-Karamany A S 2001 *J. Thermal Stresses* **24** 1159

[35] Ezzat M, Othman M I A and El-Karamany A S 2001 *J. Thermal Stresses* **24** 411

[36] Othman M I A and Singh B 2007 *Int. J. Solids and Structures* **44** 2748

[37] Othman M I A and Kumar R 2009 *Int. Comm. in Heat and Mass Transfer* **36** 513